Using Collision Cross Section Distributions to Assess the Distribution of Collision Cross Section Values

Aidan P. France, Lukasz G. Migas, Eleanor Sinclair, Bruno Bellina and Perdita E. Barran*

Michael Barber Centre for Collaborative Mass Spectrometry, Manchester Institute of Biotechnology and Photon Science Institute, University of Manchester, 131 Princess Street, Manchester, M1 7DN, UK

Abstract

Careful transfer of ions into the gas-phase permits the measurement of protein structures, with ion mobility-mass spectrometry, which provides shape and stoichiometry information. Collision cross sections (CCS) can be obtained from measurements made of the proteins mobility through a given gas, and such structural information once obtained should also permit inter-lab comparisons. However, until recently there was not a recommended standard form for the reporting of such measurements. In this study we explore the use of collision cross section distributions to allow comparability of IM-MS data for proteins on different instruments. We present measurements on seven standard proteins across three IM-MS configurations, namely an Agilent 6560 IM QToF, a Waters Synapt G2 possessing a TWIMS cell and a modified Synapt G2 possessing an RF confining linear field drift cell. Mobility measurements were taken using both He and N_2 as the drift gases. To aid comparability across instruments and best assess the corresponding gas-phase conformational landscapes of the protein 'standards' we present the data in the form of averaged collision cross section distributions. For experiments carried out in N_2, CCS values for the most compact ion conformations have an inter-instrument variability of ≤ 3%, and the total CCS distributions are similar across platforms. For experiments carried out in He, we observe the total CCS distributions to follow the same trend as observed in N_2, whilst CCS for the most compact ion conformations sampled on the 6560, are systematically smaller by up to 10%, than those observed on the G2. From this study, we observe the applied protein calibration procedure (for TWIMS) to yield ^{TW}CCS for native-like proteins which are largely similar to those obtained on DTIMS instruments. However, when considering the ease by which unintentional protein structural activation *in vacuo* can occur and the broad range of ^{DT}CCS within the literature from which to calibrate drift times against, we advise caution when calibrating sample protein drift times against protein 'standards' in order to obtain CCS values and recommend the use of CCS distributions.

1. Background & Motivation

Ion mobility spectrometry (IMS) coupled with mass spectrometry (IM-MS) permits the characterisation of an ions structure from its mobility in a gas (IM) as well providing its mass (MS).[1] IM-MS is now established as a method to interrogate the structure of proteins, and under gentle ionisation conditions ESI can produce ions which retain aspects of their solution-phase structure.[2–7] IM-MS approaches have been exploited to permit the structural and functional characterisation of many types of biomolecules, including peptides;[8,9] small monomeric proteins;[5,10] cytosolic and membrane bound protein complexes;[11,12] protein-protein and protein-ligand interactions;[13–16] Nucleic

acids[17,18] and amyloidogenic proteins.[19,20] Regardless of the molecular species to be analysed there are features or constraints that are common to all IM-MS experiments. These have recently been well outlined for all the prevalent forms of IM-MS.[21] Protein measurements have in the main utilised a form of ion mobility which can be generally described by a common process. In this, packets of ions are focussed to traverse a drift cell filled with an inert buffer gas at a known temperature and pressure (1mbar to atmospheric) whereby weak electric fields act to axially propel them through a drift cell/region. As they traverse this gas filled cell, the "frictional" force of gas-ion collisional events retards their motion, thus permitting the temporal separation of ions based upon their size, shape and charge.[22,23] IM-MS experiments record the arrival time (t_A) of m/z selected ions and this data can be used to determine their rotationally averaged collision cross sections (CCS).[24] Leading a wide community effort Gabelica recently recommended how to report IM-MS measurements to better facilitate inter-lab comparability and in this work we take this as the basis by which we can compare the data obtained on well-studied proteins.[21]

In so called, 'native' mass spectrometry experiments, a protein of interest is infused from an aqueous solution along with volatile salts such as ammonium acetate buffered to appropriate physiological pHs (~6-8).[2,25] In order to retain solvated structures *in vacuo*, careful optimisation of source parameters is necessary to minimise collisional heating and subsequent structural rearrangement.[26] Such effects can also occur on the injection of desolvated ions into the ion mobility drift tube.[27] Foundational studies from Clemmer and Jarrold demonstrated that minimising the energy of ions prior to IM separation permits the retention of native-like conformations for the monomeric proteins ubiquitin and cytochrome c.[10,28] In addition, Williams and Russell, using a 2nd generation Waters Synapt G2 ion mobility-mass spectrometer, demonstrated how voltages and trapping conditions prior to the drift cell can substantially affect the conformational landscapes of ubiquitin and metallothionein-2A.[26,29] Furthermore, Gabelica *et al*. defined tuning parameters on an Agilent 6560 IMQToF which allowed the preservation of a compact so called "N state" of Ubiquitin as well as the ammonium-bound states of a fragile nucleic acid complex.[30] Such efforts to establish optimal gentle transfer of biomolecules via careful tuning of ion optics across homemade and commercially available IM-MS instruments, have been used to support arguments about the preservation of solution-like biomolecular structures *in vacuo*, although it is evident that the ESI process also plays a major role.

Despite the body of work that reports the conditions required to 'least perturb' the structure of proteins for IM-MS measurements, there has been less focus on the reproducibility of CCS, with exceptions being studies on small biomolecule CCS on single vendor platforms.[31–33] To our knowledge, there have only been a handful of publications in which protein CCS have been compared across different platforms.[34,35] That being said, none of these studies have employed the use of CCS distributions to probe the conformational landscape of the systems under analysis. Visualising these ion conformational landscapes for malleable systems has great utility in defining optimal tuning parameters for native IM-MS experiments and as such, is commonly employed within many labs including our own.

In this study we establish "starting point" operational parameters which minimise the gas-phase activation of proteins across three instrumental platforms. We report CCS distribution/CCS across three ion mobility-mass spectrometers: the Synapt G2 (TWIMS & RF DTIMS configurations) and the Agilent 6560, in helium and nitrogen drift gases, to ascertain the degree of differentiation between protein structures sampled across different IM-MS platforms under "soft" tuning conditions. In addition, we provide interactive representations of CCS distributions to augment traditionally numerical CCS datasets. Furthermore, we present global CCS histogram distributions for

compiled literature CCS values of our chosen systems, in order to facilitate a better understanding of where individual "native IM-MS" CCS lie relative to previously published values.

2. Methods and Materials

2.1. Sample preparation and ionisation

Seven commercially available protein/protein complex standards were utilised for the experiments outlined in this study. Sample identities, sources, suppliers, catalogue numbers and final solution conditions are detailed in SI Table S1.

Ammonium acetate solutions were made by dissolving ammonium acetate (Sigma) in ultrapure water (Merck Milli-Q) to yield ionic buffer concentrations of 50 or 200 mM (SI Table S1). All of these solutions were then adjusted to a pH of 7.4 using ammonium hydroxide solution (Sigma).

All seven samples were purchased as lyophilised powders which were dissolved in either 50 or 200 mM ammonium acetate solution, pH 7.4, to form protein stock solutions (typically 100 µM protein concentrations). These stocks were then de-salted twice using Biospin-6 columns (BioRad, USA), aliquoted out, flash frozen and stored at -80 °C until the day of analysis. On the day of analysis, aliquots were thawed at r.t and diluted to their final concentration prior to experimentation (SI Figure S1).

A mixture of commercially available phosphazine salts pre-dissolved in a acetonitrile/water solution (95:5, % v:v) (G1969-85020) known as "tunemix" (Agilent technologies, Santa Clara, CA), as well as poly-DL-alanine (Sigma, P9003) and myoglobin (Sigma, G7882) dissolved in water/methanol/formic acid (50:50:0.1, % v:v) were used to optimise the helium IM-Trap differential on the modified Agilent 6560 IMQToF.

All experiments were performed using nano-electrospray ionisation (nESI) in positive ionisation mode. Samples were infused into emitters prepared in-house from thin walled (O.D. 1.2 mm, I.D. 0.9 mm; WPI, UK) and thick walled (O.D. 1.2 mm, I.D. 0.69 mm; Sutter Instrument Company, USA) fire polished borosilicate glass capillaries using either a Flaming/Brown P-97, Sutter P1000 or P2000/F micropipette puller (Sutter Instrument Company, USA). In order to facilitate more facile spraying, all solution loaded emitters were centrifuged at 5000 rpm for 15 seconds prior to loading into the instrument tip holder. Platinum wire (diamater 0.125 mm, Goodfellow Cambridge Ltd, UK), was inserted into the capillaries to permit efficient ionisation. In order to compensate for the reduction in ion transmission which typically accompanies native IM-MS instrument optimisation, all experiments were carried out in sensitivity mode.

2.2 Instrumentation

2.2.1. Waters Synapt G2 (TWIMS)

Travelling wave derived CCS distributions/CCS were obtained on a Synapt G2 (Waters, UK) with nitrogen as the drift gas (SI Figure S2). Within this instrumental configuration, ions can be mass selected in the quadrupole prior to IMS. After navigating the quadrupole, ions enter the "Tri-wave" region which encompasses: 1) an argon filled trap cell, where ions are periodically stored and gated into the helium cell, 2) a helium cell held at a comparatively high

pressure to the trap cell, where ions experience "collisional cooling" prior to IM separation, 3) an ~25 cm long TWIMS cell filled with nitrogen, whereby propagating DC waves enable the mobility separation of ions based upon their size, charge and conformation and 4) a transfer cell which acts to ferry ions toward the ToF analyser for *m/z* quantitation. For all the TWIMS experiments within this study, IM wave velocities of 100-300 ms^{-1} and wave heights of 9.5-19.5 V were employed. General parameters employed for native TWIMS experiments are outlined in Table S2. For a more detailed description of the Synapt G2 (TWIMS), see Giles *et al.*[36].

2.2.2. Waters Synapt G2 (DTIMS)

The Synapt G2 was modified *via* substitution of the travelling-wave IM cell (incorporating the helium cell) with an ~25 cm long RF-confining drift cell (Waters, UK) (SI Figure S3).[37] Helium/nitrogen gas was introduced into the RF cell using a gas inlet system positioned in the centre of the cell to promote pressure homogeneity (SI Figure S4). Absolute IM cell pressure readouts were enabled by the installation of a baratron (model 626C, MKS, UK). Drift gases could be switched by toggling the "He" (for helium) or "IMS" (for nitrogen) tabs, whilst the RF confining drift cell could also be operated using the original instrument software (MassLynx V4.1) (SI Figure S4). The static potential gradient required for IMS was applied across the RF cell using a combination of four DC voltages (SI Figure S3). For all the experiments outlined in this study, six drift voltages separated by 25 V increments were employed to obtain ion dead times (t_0) and subsequent CCS/CCS distributions. It is important to note that the RF cell pressure was left to equilibrate for >30 minutes after gas initiation/switching prior to data acquisition. General parameters employed for native DTIMS experiments performed on the modified G2 are outlined in SI Table S3. For a more detailed description of the modified Synapt G2 (DTIMS), see Allen *et al.*[37].

2.2.3. Agilent 6560 IMQToF

The setup employed for helium and nitrogen experiments carried out on the 6560 is described in SI Figure S5. For experiments undertaken on the 6560, an orthogonally configured nESI source (G1988-60000 Nanospray, Agilent) was utilised. The source drying gas flow (nitrogen), which was observed to have a large impact upon the observed analyte charge state distributions (CSDs) (SI Figure S6), was adjusted to below 2 L min^{-1} by a manual flow controller (Porter instrument company, USA) fitted to the drying gas outlet and source inlet. Post source, ions were transferred through a heated capillary into a two-stage ion funnel, the first of which focuses ions *via* the use of elevated pressures, whilst the latter operates as an ion funnel trap which enables the release of discrete ion pulses into the IM cell. The IM region comprises an ~78 cm long static field drift tube with an absolute pressure capacitance gauge (CDG 500, Agilent) positioned at the far end of the cell and a thermocouple (Type K, Omega engineering) positioned above the middle of the cell. The instrument configuration employed for measurements taken with nitrogen and helium drift gases is depicted in SI Figure S5. For measurements taken in nitrogen, a positive IM cell pressure differential of 0.15 Torr relative to the preceding trapping funnel was utilised, as described previously.[38] The pressure differential was maintained within 0.01 Torr *via* the inclusion of a drift gas kit (G2582A, Agilent) fitted with a precision flow controller (640B 10 Torr range, MKS) which regulated drift tube pressure by responding to the absolute pressure capacitance gauge (CDG 500, Agilent). However, we found the precision flow controller to be unable to maintain pressure differentials when the instrument was operated with helium as the drift gas. As such, we modified the gas inlets into the trap and IM cell so as to bypass the flow controller and permit manual control of the gas pressures using needle valves (Swagelok) (See SI Figure S5). After carrying out pressure differential

optimisation experiments in helium using tunemix (SI Table S4), polyalanine (SI Table S5) and myoglobin (SI Table S6), we settled on an optimum helium IM-Trap differential of ~0.13 Torr. This differential prevented nitrogen contamination in the IM cell, resulting in $^{DT}CCS_{He}$ values closest to those previously published. It is important to note that all gases pass through a gas purifier trap (nitrogen and helium; RMSN and RMSH, Agilent) prior to entering the instrument in both of the instrumental configurations employed. Data was recorded using the MassHunter Data Acquisition software (Agilent) using the stepped-field method, whereby incremental variation of the electric field (five 100 V steps) across the drift cell permitted enumeration of the CCS distributions for a given ion. General parameters employed for native experiments performed on the 6560 IMQToF are outlined in SI Table S7. For a more detailed description of the 6560 IMQToF, see May *et al.*[39].

2.3. Data Analysis and CCS distribution production

All experimental data obtained from the Synapt G2 (with TWIMS/DTIMS configurations) was analysed using MassLynx V4.1 software (Waters, UK). Arrival time distributions (ATDs) encompassing a drift time axis (x-axis) and an associated ion intensity axis (y-axis) were extracted for the desired *m/z* region (Figure 1 a. ii). The drift time axis was transformed to a CCS axis by employing suitable calibrant ions (SI Table S8) following an approach described previously for TWIMS,[11,40,41] or DTIMS data (Figure 1 a & b iii & iv).[23,42] Data acquired on the 6560 IM-QToF was analysed using MassHunter IM-MS Browser software (Agilent). Drift times and their corresponding ion intensities were extracted for the desired *m/z* regions (Figure 1 b. ii), as for data acquired on the Synapt G2. However, unlike MassLynx software, the MassHunter IM-MS browser records all IMS parameters, these can then be extracted as tabulated data and applied to the Mason-Schamp equation to convert the x-axis from drift time to CCS units (Figure 1 b. iii & iv).

Each replicate yielded a single CCS distribution plot with slightly different x-axis CCS binning increments (due to different A and X values from TWIMS experiments and different dead times in DTIMS experimental replicates) (Figure 1 b. iv. Top). In order to produce averaged CCS distribution plots from individual CCS distribution replicates, Gaussian fits were made to the experimental data using a consistent number of data points (e.g. 1000) across a fixed CCS range (e.g. 2500-4500 $Å^2$). After fitting all CCS distribution replicates for a single ion across the same CCS range and number of data points, the average CCS distribution plot was constructed as follows: 1) The range employed for the CCS distribution replicate was extracted and used to form the x-axis of the averaged CCS distribution plot. 2) The ion intensity across the CCS range of each replicate was averaged whereby standard deviations denote the variation between replicates. 3) The constructed x-axis, y-axis and y-axis standard deviation were combined to obtain averaged CCS distributions (Figure 1 b. iv. Bottom). Ion CCS were obtained *via* averaging apex values from Gaussian fitted CCS distribution replicates. Associated CCS errors (±) came from the standard deviation of these values. Total CCS distribution plots for protein/protein complexes were obtained by combining averaged ion CCS distribution plots (normalised for mass spectral peak intensity and CCS distribution area). All CCS distributions produced within this study were constructed using OriginPro 2015/2017 software.

2.4. Interactive figures

A number of main text and SI figures presented in this article were recreated in an interactive format to enable in-depth interrogation of the presented results. These are deposited online at https://france-ccs-2019.netlify.com/.

The interactive figures were created using ORIGAMI[ANALYSE] and require the use of a modern internet browser and access to the internet.[43]

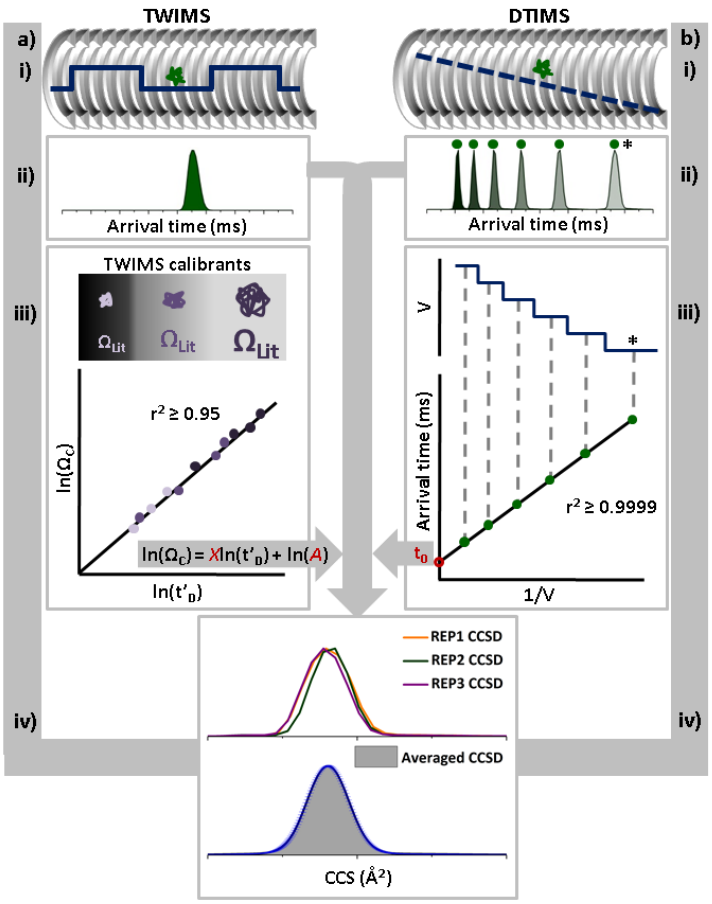

Figure 1. Schematic showing how TWIMS (LHS) & DTIMS (RHS) data yields averaged ion CCS and CCS distributions. a) i) Schema for the trajectories of ions in each type of IM experiment. ii) Example ATDs required to determine CCS distributions. For DTIMS data (RHS) the ATD corresponding to the lowest DV is marked by (*). iii) LHS: Drift times from calibrant ions with previously measured ^{DT}CCS which bracket the mass of the ion of interest are corrected for their charge, time spent outside the drift cell post IM and reduced mass, yielding a plot that converts experimental corrected drift times (t'_D) to CCS (Ω_C). From the plot of $\ln(\Omega_C)$ vs $\ln(t'_D)$, the exponential factor (X) and fit-determined constant (A) can be obtained for conversion of ATDs into CCS distributions. RHS: The arrival time apex of ions obtained from each DV are plotted against a reciprocal of the DVs (1/V), where the y-intercept of this plot yields the ion 'dead time' (t_0), which is the time spent outside of the drift cell. Additionally, the slope of the plot represents the ions mobility. iv) CCS axes are not the same across CCS distribution replicates, so interpolation of the data yields an averaged CCS distribution wherein error bars (blue) represent the deviation between replicates.

3. Results and Discussion

3.1 Tuning ion transmission to preserve structure

Native IM-MS workflows are dependent upon the solvation of biomolecules within non-denaturing, MS compatible solutions which adequately reflect the electrolytic milieu of the cell.[25,44,45] Accordingly, aqueous ammonium acetate

adjusted to pH (~7) is the most commonly employed solution for native IM-MS experiments.[25,44,45] In order to sample macromolecular structures which most closely resemble those found in physiological solutions, IM-MS instrumentation has to be carefully tuned so as to reduce lab frame energies and in turn, ion internal energies (E_{int}) which promote gas-phase restructuring.[26] Perturbations in protein conformation, *via* ion heating, often have minimal effects upon the observed CSD (Figure 2a insets);[26] as a result, structural conclusions derived solely from protein charge state signatures (i.e CSDs) observed *via* native MS should be addressed with caution.[46,47]

To ascertain the degree to which a set of instrument parameters promote ion activation, we use the observed ATD of selected proteins as a measure of transmission 'softness', analogous to the use of fragments from thermometer ions.[29,48,49] Given this approach, suitable ions are those with a well-documented "native" globular state and defined unfolding pathway previously observed with IM-MS. Accordingly, we recommend the $[Ubiquitin+6H]^{6+}$ and $[Cytochrome\ c+7H]^{7+}$ ions as suitable (Figure 2a).

Post ionisation, optimisation for 'soft' ion transmission is dependent upon: 1) the reduction of accelerating voltages and 2) the modulation of gas pressures, both of which act in synergy to minimise the energy of ion-neutral collisions. In the instance where desirable 'soft' tuning has been achieved, the ATD of the thermometer ion (cytochrome c in this instance) should present with a comparatively narrow, Gaussian-like peak (indicative of a single conformational population) observed at low arrival times (Figure 2a, Top). These observations would likely point to the retention of a folded form of the protein which effectively is a dehydrated solution-phase structure; this hypothesis can be confirmed *via* CCS determination.[50] The associated mass spectrum (Figure 2a, Top, inset) presents with a dominant 7+ peak and a small amount of the 6+ ion. This mass spectrum is typical for cytochrome c sprayed from non-denaturing solutions.[51] Critical to our workflow is the observation that when certain ions undergo collisional heating, they first anneal into highly collapsed structures prior to unfolding. These collapsed structures will present in much the same manner as the native-like dehydrated ion, except with lower CCS values. Subsequently, in situations where gas-phase annealing to collapsed structures is suspected, it is instructive to compare the associated CCS with those found within the literature.[52]

For many commercial mass spectrometers the default settings employ greater accelerating voltages in tandem with gas pressures which permit increased gains in ion transmission (~5 fold) and detection efficiency. Often these gains in signal intensity are concomitant with a reduction in salt adducts (observed *via* MS). Under default settings a protein will undergo a degree of gas-phase restructuring, typically yielding more complicated ATDs (Figure 2a, Middle). Interestingly, within the corresponding MS (Figure 2a, Middle, Inset), under such conditions we observe an slight increase in the relative abundance of lower charge states (6 & 5+) when compared to the soft tune, perhaps attributed to the loss of counterions. If accelerating potentials within the instrument are increased further still, then the intermediary conformations largely re-organise to an extended gas-phase form which tends to have one conformer.[10,53] This capability to manipulate the structure of a given ion *in vacuo* is exploited in activated ion mobility (aIM)/ collision induced unfolding (CIU) experiments, which describe the gas-phase restructuring of an ion, often induced by high energy gas-ion collisions, monitored via IM-MS.[43] aIM/CIU has played a pivotal role in the interrogation of protein unfolding mechanisms as well as the effect of ligand/co-factor binding upon protein stability.[26,54,55]

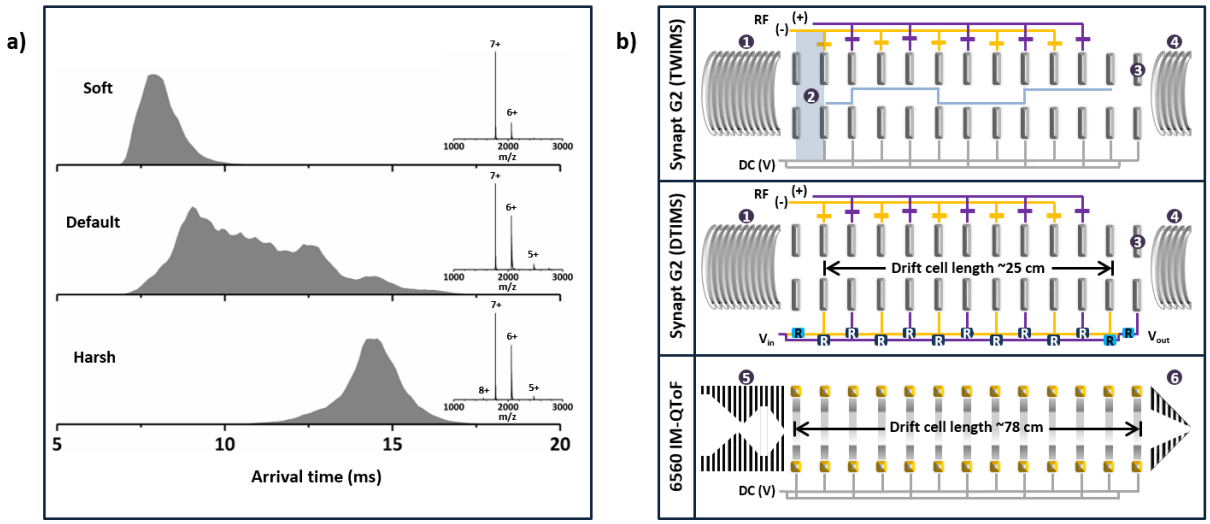

Figure 2. a) IM conformational landscapes of [cytochrome c +7H]$^{7+}$ obtained from the Synapt G2 (TWIMS) under different tuning conditions. Top) 7+ ATD observed under 'soft' settings. Middle) 7+ ATD observed under 'Default' settings. Bottom) 7+ ATD observed under 'Harsh' settings. Insets) Mass spectra corresponding to each set of tuning conditions. b) Schematic of the three IM-MS configurations employed within this study illustrating the differences in the trapping regions prior to injection to the drift cells. Top) G2-TWIMS configuration - Ions are gated from the trap region (1) into the He cell (2) where they are 'collisionally cooled' prior to reaching the IM cell. Upon entering the IM cell, ions are separated by propagating DC waves (blue line) which propel ions through the stacked ring ion guide (SRIG) filled with an inert drift gas. Ions then reach the transfer DC entrance (3) after which they enter the transfer cell (4) prior to entering the ToF-MS for *m/z* quantitation. Middle) G2-DTIMS configuration - In this setup, the helium cell entrance plate & TWIMS cell have been replaced by a linear drift cell.[37] RF-confinement of the ion beam within this configuration is established by a dual series of 330 pF capacitors. Ions traverse a uniform DC voltage gradient established via a network of resistors ('R' Boxes). Bottom) 6560 IMQToF – The trapping funnel (5) permits the temporal release of ions into the drift cell where they drift under the influence of a shallow DC potential (without RF confinement). After which the ion beam is axially refocused by the rear funnel (6) at the exit of the drift cell prior to entering the post-IM optics.

To least perturb the ions structure, its kinetic energies must be kept at or near the minimum threshold required for successful transmission. On the Synapt G2, parameters such as the trap cell gas flow, trap bias DC (which acts as an injection voltage) and Trap CE, are critical determinants of transmission 'softness' (Figure 2b, Top & Middle). The trap cell gas flow, when tuned with voltages within the trap cell, permits effective trapping of ions prior to gating into the IM region. In addition, this gas collisionally focuses ions by dampening their axial and radial velocities, which in turn increases overall ion transmission. That being said, if the trap cell flow is too high, then structural perturbation can occur due to the increased ion-gas collision frequency. In the G2 TWIMS configuration, the addition of a gas cell before the drift region (2) which acts to permit higher IM resolution, offers another parameter to alter, that of the helium gas within it.[36]

Raising the trap bias DC increases the potential difference between the trap and IM region of the G2 instrument which effectively imbues ions with greater kinetic energies as they enter the IM cell (SI Figure S2 b). Raising the Trap

CE, as with aIM experiments, acts in much the same way. Even for stable protein complexes, for example the tetrameric alcohol dehydrogenase, large potential differences applied between the trap and IM regions result in individual subunit unfolding (Figure 3a) prior to the ejection of highly charged monomers.[56,57] When modulating the trap bias DC it is crucial that a compromise between transmission 'softness' and signal intensity/MS resolution is struck, as this parameter significantly effects MS resolution and ion transmission. Surprisingly for the Synapt G2 (DTIMS configuration), we also found the trap wave height (WH) has an observable impact upon the conformational landscape sampled for monomeric protein ions. We believe this affect to be due to the increased kinetic energy imparted upon ions within the trap when higher trap WHs are employed. Interestingly, we did not observe this effect on the Synapt G2 (TWIMS configuration). In agreement with Williams *et al.*[29], we did not observe TWIMS wave velocity or wave height to have any observable effect upon the conformational landscape sampled for any of the ions analysed. Voltages at the beginning of the IM cell, namely the IMS entrance voltage and the He cell DC (Figure 3a), were also observed to have a 'fine tuning' effect on the observed ion ATD (for monomeric proteins), with the latter only impacting the ATD when the G2 was configured for TWIMS.

In contrast to the aforementioned pre-IM DC voltages, variation of RF voltages within both instrument configurations were not observed to have any significant effects upon ion ATDs, although they did have a notable impact upon ion transmission.[58] To offset reductions in ion transmission which occur under native IM-MS settings, the IM bias DC, transfer CE and transfer wave velocity can be raised. Increasing the IM bias DC and/or the transfer CE, raises the potential energy difference between the IM and transfer region and thus raises ion kinetic energies post-IMS (SI Figure S2b). Optimisation of these three parameters permit favourable gains in ion transmission concomitant with the dissociation of non-volatile salt adducts.

Tuning for 'soft' ion transmission on the Agilent 6560 IMQToF, like the Synapt G2, is largely dependent upon the application of voltages within the trapping region (Figure 2b, Bottom). Most importantly the trap entrance grid delta, which is the potential difference between the trap during filling (low) and during storage and release (high), had a significant effect upon ion activation. This effect was most notable for small monomeric proteins such as cytochrome c (Figure 3b) and was in corroboration with findings from Gabelica *et al*.[30]. Unlike the Synapt G2, we observed tuning of the RF voltages within the 6560 to have a noticeable effect upon ion activation (Figure 2b). The most significant of these was the trapping funnel RF which acts to radially confine ions within the trapping funnel prior to gating into the IM cell. In contrast to Gabelica *et al*.[30] and Mclean *et al*.[51], we found that maintaining the trap DC voltages employed across both N_2 and He drift gases (SI Table S7) did not yield any observable differences in protein conformation (See SI Figures S7-20, LHS column). Within the source region of the instrument we observed minor effects on the conformation of monomeric proteins when the fragmentor voltage, was altered within the 300-400 V range. Lower fragmentor voltages led to losses in signal transmission without gains in transmission 'softness', whilst higher fragmentor voltages did not permit gains in signal intensity yet began to promote ion activation.[30]

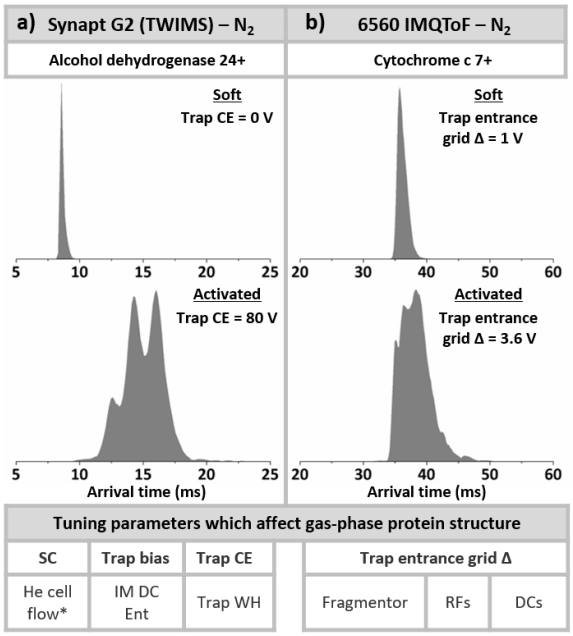

Figure 3. The use of alcohol dehydrogenase and cytochrome c (200 mM and 50 mM AmAc solutions respectively) to illustrate the effect of altering instrument parameters a) [Alcohol dehydrogenase + 24H]$^{24+}$, Synapt G2, Top) soft tuning, whereby no trap collision energy is applied. Bottom) activating tuning: trap collision energy has been raised to 80 V. b) [Cytochrome c + 7H]$^{7+}$ 6560 IM-QToF, Top) soft tuning parameters: gating height of the trap entrance is +1V. Bottom) using activating tuning parameters: whereby the gating height of the trap entrance is +3.6V. The table describes the parameters which we have found to have substantial (grey & bold) and lesser (just grey) affects upon ion activation on the Synapt G2 (LHS) and 6560 IMQToF (RHS). (*) G2-TWIMS configuration only. SC = source cone potential for the G2.

3.2 Assessing inter-instrument variation in the CCS distributions for proteins and protein complexes

After 'soft' and comparable ion transmission parameters were defined across the three instrumental platforms, we focused upon the IM-MS analysis of a range of protein analytes that are readily available and have been much studied before (Table S1). We sought to compare analyte gas-phase CCS distributions with both He and N_2 as drift gases (SI Figure S7-20). In Figure 4 we compare the data obtained for tetrameric concanavalin a with cytochrome c. Concanavalin a presents with a CSD centring on the 20+ species and a Δz of 5 (although the charge states at either end of the CSD are often barely visible). Across all three instruments, the CCS distributions for the tetrameric species of concanavalin a largely present as unimodal Gaussian-like peaks which yield CCS_{He} values (replicable to within ~0.5%) that differ by ~0.1-0.9% across charge states and <2% across instruments (when comparing like charge states).

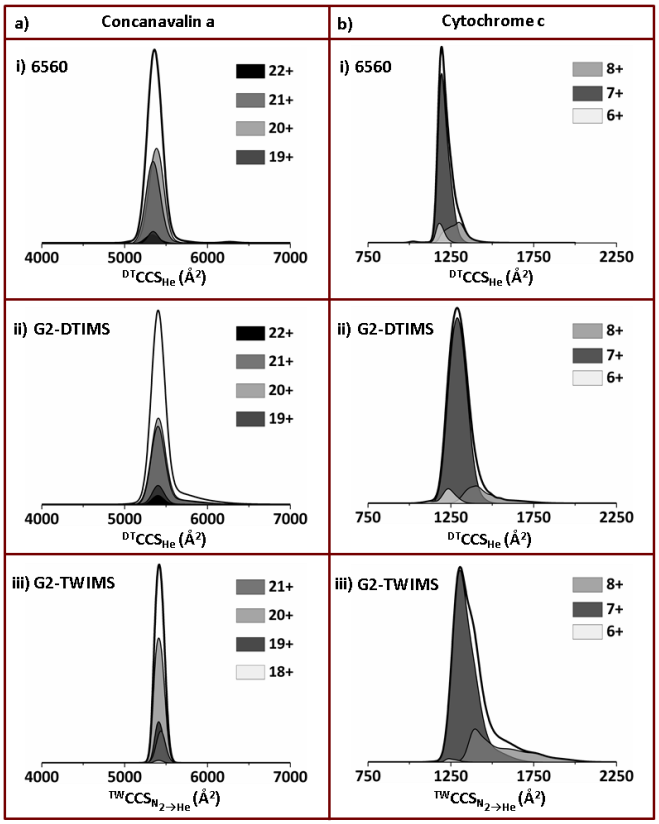

Helium CCS values (Å^2) across all platforms

Concanavalin a			
Z (+)	6560	G2-DTIMS	G2-TWIMS
18	-	-	5412 ± 16
19	5340 ± 15	5399 ± 2	5409 ± 8
20	5384 ± 20	5397 ± 1	5412 ± 14
21	5345 ± 29	5401 ± 1	5434 ± 18
22	5335 ± 23 6285 ± 24	5405 ± 1	-

Cytochrome c			
Z (+)	6560	G2-DTIMS	G2-TWIMS
6	1182 ± 4	1234 ± 5	1238 ± 6
7	1196 ± 1	1286 ± 12	1304 ± 6
8	1258 ± 19 1297 ± 2	1373 ± 34 1540 ± 17	1399 ± 6 1625 ± 11 1768 ± 6 1918 ± 12

Figure 4. Total CCS distribution for a flexible protein and rigid protein complex obtained across all instrumental platforms utilised within this study with helium as the drift gas. a) Total CCS distributions obtained when analysing monomeric cytochrome c using parameters tuned for native IM-MS on the i) Agilent 6560 IMQToF, ii) Synapt G2 (TWIMS) and iii) Synapt G2 (DTIMS). b) Total CCS distributions obtained when analysing tetrameric concanavalin a using parameters tuned for native IM-MS on the i) Agilent 6560 IMQToF, ii) Synapt G2 (TWIMS) and iii) Synapt G2 (DTIMS). The total CCS distribution trace encompassing the averaged CCS distributions for each analyte charge state are represented by the thick black lines. The colours of the CCS distributions for each charge state observed correspond to the key at the RHS of each total CCS distribution. The table underneath the total CCS distributions describes the average CCS_{He} values obtained for the observed conformations of concanavalin a (LHS) and cytochrome c (RHS) across the three instrumental configurations employed. The (±) values represent the standard deviations across replicates. For all of these experiments concanavalin a and cytochrome c were sprayed from 200 mM and 50 mM AmAc solution (pH 7.4) respectively.

Our findings suggest that we are probably sampling a single conformational population which is retained across the charge states analysed, as might be expected for a well-structured protein complex. The only exception to this is the

$[M+22H]^{22+}$ species which presents as a bimodal CCS distribution with a larger conformer observed at ~6300 Å^2 (SI Figure S17). Previous aIM experiments on concanavalin a, showed a larger species with a drift time which was ~25% higher than the structure sampled prior to activation.[43,59] Regarding the CCS distribution for concanavalin a analysed in He, the charge states sampled on a given instrument possess almost identical widths (with the exception of the 19+ species sampled on the 6560 which is notably narrower) (SI Figure S17). However, across instruments there are observable differences in CCS distribution width. Most notably the CCS distributions obtained from the G2 (TWIMS), both for N_2→He (SI Figure S17) and N_2 (SI Figure S18) are ~50% narrower than the corresponding CCS distributions obtained from the 6560 and G2 (DTIMS) respectively, which themselves are very similar to one another (Figure 4a). With nitrogen as the drift gas, we observe predominantly unimodal Gaussian-like CCS distributions (as in He) but with CCS (replicable to within ~0.5%) that differ more significantly across charge states (~0.9-4.3%) but not instruments (<2%) (SI Figure S18). For clarity we have provided representative raw ATDs to show the unprocessed gas-phase conformational landscapes we observe by IM in both He (SI Figure S21) and N_2 (SI Figure S22), within this study. The most notable variation across CCS_{N_2} values is observed on the G2-TWIMS, where the highest charge state (21+) is ~4.3% bigger than the lowest charge state (18+). This difference is most likely due to the Ω_{Lit} values employed for the $^{TW}CCS_{N_2}$ calibration procedure. In accordance with this hypothesis, a significantly smaller CCS variation across charge states is observed (~0.5%) for the same raw data set calibrated to yield $^{TW}CCS_{N_2\rightarrow He}$ values. In contrast, the range of CCS_{N_2} values obtained for concanavalin a on the G2 (DTIMS) and 6560 do not vary to the same degree, at ~1.7 and 0.9% respectively.

Cytochrome c also presents as a narrow CSD, with a Δz = 2-3, centring on the $[M+7H]^{7+}$ species (Figure 2 and SI Figure S9). Across all three instruments, the ATDs for the $[M+6H]^{6+}$ are bimodal, but here the earlier arriving species corresponds to a concentration specific coincident dimer whilst the $[M+7H]^{7+}$ ATD is unimodal. Slight tailing toward higher CCS is observed for the $[M+6H]^{6+}$ on the G2 (TWIMS) and the 7+ ion analysed on the 6560 and G2. The CCS distribution of the 7+ ion, analysed on the G2 is comparatively broad (Figure 4 & SI Figure S9). This tailing and broader CCS distribution (7+, G2) may be indicative of a lowly populated, partially unfolded conformer which we were unable to resolve. In contrast to the highest charge states of concanavalin a, the 8+ species of cytochrome c when sampled on the G2 presents as a broad unresolved peak with one dominant, partially resolved apex with a notable tail. This tail likely constitutes numerous unresolved, closely related intermediate conformations resulting from differing degrees of structural activation. On the other hand, the 8+ ion sampled on the 6560 presents as a far narrower, albeit partially resolved peak with minimal tailing. Across the three instruments, the CCS_{He} values for the most compact ion conformations observed vary by ~0.3-9%, with the variation increasing with increasing charge (Figure 4 & Figure 5). However, most of this variation is due to the CCS_{He} values obtained on the 6560 which are ~4-9% smaller than those obtained on the G2 platform. When comparing CCS_{He} values obtained on the 6560 and G2 we observe the same trend (to differing degrees) for all analytes within this study, except for concanavalin a (Figure 5). Interestingly, the systematic reduction in measured CCS on the 6560 relative to the G2 is not observed with nitrogen as the drift gas (SI Figures S7-S20 & S23). Comparing the total CCS distribution plots for cytochrome c across the three instruments employed, we see that the CCS distribution widths, particularly for the 7+ and 8+ ion, are considerably wider on the G2 platform (~50%) than on the 6560. This finding is inconsistent with the total CCS distributions of concanavalin a, where the opposite is observed.

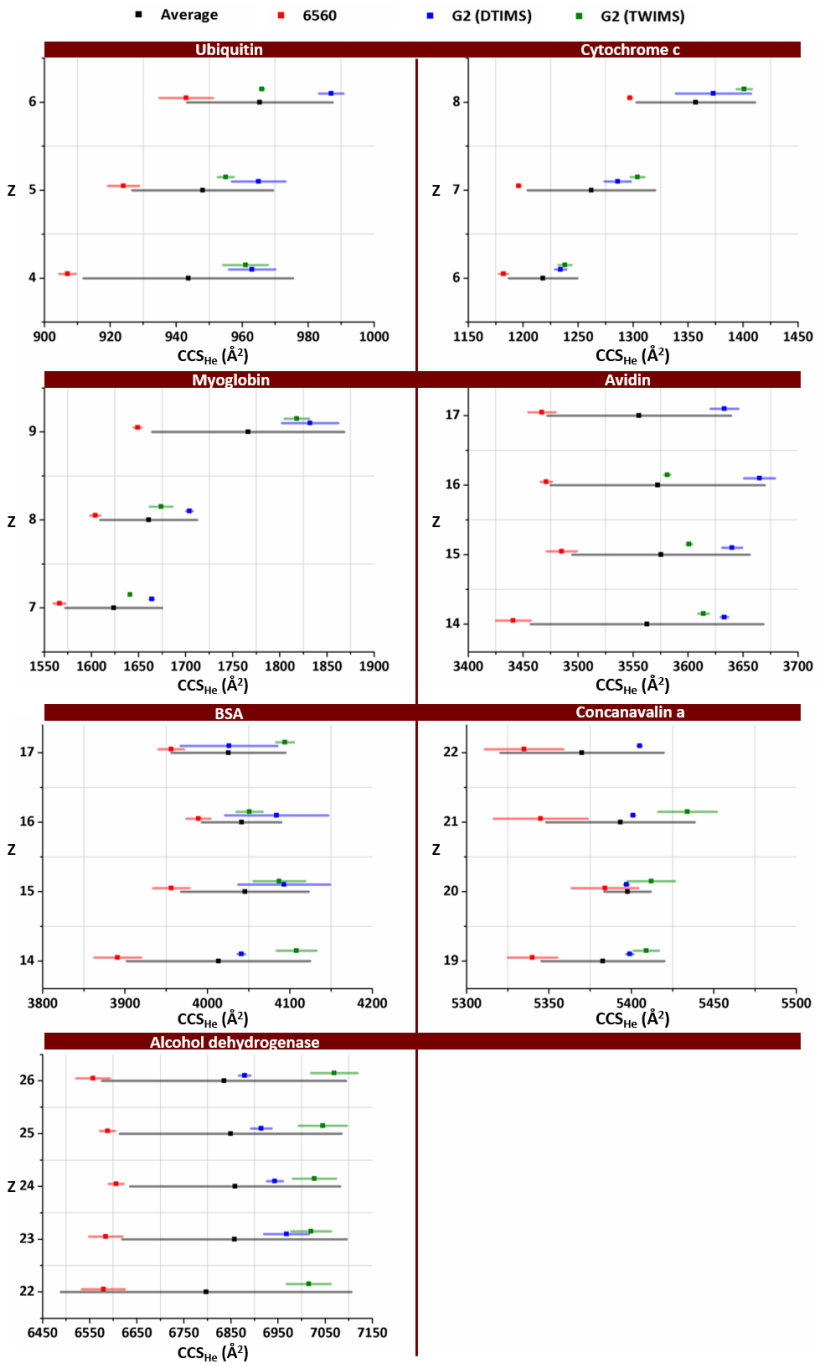

Figure 5. Scatter plots showing the range of CCS_{He} values obtained for the protein/protein complexes analysed within this study across the instrumental platforms utilised. In all cases the CCS for the single most abundant conformation for each charge state was compared across the three instruments. The black, red, blue and green squares represent the average CCS_{He} values obtained for single conformations as an average across all the instruments, on the 6560, the G2 (DTIMS) and the G2 (TWIMS) respectively. The associated coloured bars show the standard deviation across the experimental replicates.

3.4 Comparisons with literature

In order to visualise the general spread of conformations for proteins/protein complexes across the literature, as well as this study (as discussed above), we have plotted all of the CCS values we could find, for all the analytes and their charge states observed in this study, as global CCS frequency histogram plots (see Figure 6 for cytochrome c [He & N_2] and SI Figures S24-S35 and Tables S9 & S10 for all of the analytes). These plots, along with their associated tabulated CCS should act as a rough guide for future native IM-MS analyses of the analytes discussed within this study.

The CCS_{He} values obtained for the 6+ and 7+ ions of cytochrome c within our study are ~6% smaller to 5% larger than the most compact conformations sampled by Clemmer and co-workers on their 50.6 cm and 7.6 cm long drift tube instruments (Figure 6a & Table S9).[10,60,61] Additionally, our CCS_{He} values are ~ 8 % smaller to 2 % larger than those measured by Bush *et al*. on a modified Synapt G2 with an RF confining linear cell (Figure 6a & Table S9).[37,41] Regarding the most compact conformations of the 8+ ion sampled on the G2 our CCS_{He} values are ~9-12% larger than those reported by Clemmer, whilst the values obtained from the 6560 are <1% larger than the most compact conformation sampled by Clemmer (Figure 6a & Table S9).[10,60,61] Furthermore, our measurements for the most compact conformations of the 6+, 7+ and 8+ ions range from 5-21% smaller than the most compact conformations sampled by Mclean *et al*. on a 6560 IMQToF (Figure 6a & Table S9).[51] Importantly, our measurements on the 6560 in He, are seen to provide the largest source of variation when comparing our CCS_{He} values with those found in the literature.

The CCS_{He} values measured for concanavalin a within this study are in good agreement (~0.5-3% smaller) with those obtained on a modified Synapt G2 (RF confining linear cell) by Bush *et al*.[37,41], and those measured on a home built VT-IM-MS instrument by Barran *et al*. (SI Figure 32 & Table S9).[62] That being said, Barran *et al*. also recorded CCS, on a home-built IMQToF, which were ~8-18% smaller than those observed in our study (SI Figure S32 & Table S9).[52,63] Regarding the small body of published CCS_{N_2} measurements, the values we have obtained within this study are systematically smaller (~0.5-4%) than those measured by Bush and coworkers on a 1st and 2nd gen RF confining drift cell and on a SLIM system (SI Figure S33 & Table S10).[41,64]

When comparing our CCS_{N_2} values with those obtained in the literature, our values for the 6+ and 7+ ions of cytochrome c are systematically smaller than the most compact conformers obtained in a series of studies by Bush *et al*. by anywhere from ~1 up to 25% (Figure 6b & Table S10).[41,64] In comparison to measurements by Mclean *et al*. on a 6560 IMQToF, our measurements range from 5-13% smaller for the 8+, 4 % smaller to 2% larger for the 7+ and 7-8% larger for the 6+ ion (Figure 6b & Table S10).[51] We reason that the most compact conformation measured for the 6+ ion by Mclean *et al*. corresponds to a trace amount of coincident dimer, which, if we were to measure as a compact conformer of the 6+ ion (as an average across the three instruments utilised), does yield a CCS_{N_2} of 1326 ± 48 Å^2 which is in close agreement with their published CCS_{N_2} value of 1360 ± 13 Å^2.[51] Accordingly, our measurements for the 6+ ion are <1-2% smaller than the measurement given for the most abundant conformer they observe, making it more likely that this species is indeed the most compact conformation of the 6+ ion which they sampled. The above information, together with prior EHSS and PSA models (in He) for the native fold of cytochrome c, suggest that for the 6+, 7+ (on all instruments) and 8+ ion (measured on the 6560), we are sampling dehydrated, partially

collapsed, native-like structures of cytochrome c.[10,51,65] Regarding the 8+ ion, the conformations sampled on the G2 likely represent different intermediates along the gas-phase unfolding pathway toward more extended structures, as seen previously.[10,66] In contrast, concanavalin a does not show the same degree of charge/instrument dependent CCS distribution variation and CCS increase, likely due to its more rigid structure.

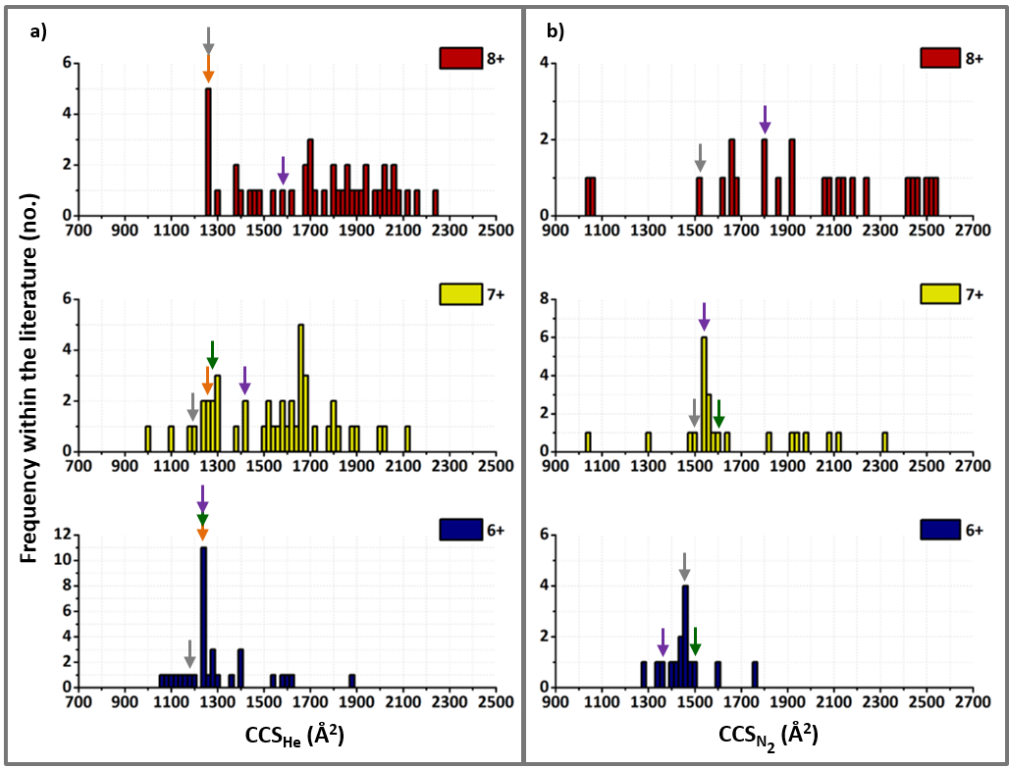

Figure 6. Global histogram plots of cytochrome c. a) Global CCS_{He} histogram plots, b) Global CCS_{N_2} histogram plots, for all the experimentally observed charge states of cytochrome c. Literature as well as our own experimentally obtained CCS values were grouped into 20 Å^2 bins, whereby the frequency of CCS values to the nearest 20 Å^2 increment were summed and represented as solid bars within the histogram plots. Within these stacked histogram plots, blue, yellow and red bars represent the frequency and size of CCS values for the 6+, 7+ and 8+ ions of cytochrome c respectively. Grey, orange, green and purple arrows represent the smallest CCS values measured from this study, and the literature values of Clemmer *et al*., Bush *et al*. and McLean *et al*. respectively.[10,41,51,60,61,64]

Across all of the protein/protein complexes analysed, we present CCS_{N_2} values which are reproducible to within <3 % across the 6560 and G2 (TWIMS and DTIMS) configurations. Similarly, this degree of variation was observed when comparing CCS_{He} values obtained across both configurations of the G2. However, CCS_{He} values derived from the Agilent 6560 proved significantly different to those obtained on the Synapt G2 platform, with the (notable) exception of concanavalin a. If this difference in CCS was a result of applying an incorrect IM-Trap pressure Δ, then we would expect 1) The CCS_{He} values obtained for the monomorphic test systems utilised to be significantly different from their published values and 2) all of the CCS_{He} values to be systematically larger on the 6560 relative to the G2, as the drift cell would be contaminated with nitrogen gas (if the IM-Trap pressure Δ was too low), which would retard ion motion more than helium, leading to comparatively longer drift times and thus larger CCS.[51] Instead, at a

Δ of ~0.13 Torr, we observe the CCS_{He} values for the monomorphic systems to be in close agreement with the average helium CCS derived from previously published data (<0.5%).[27,37,51,67–70] In addition, the CCS_{He} values for the analytes under test were systematically smaller than those observed on the G2, by an average of 4.3% and a maximum of ~ 10 %. As we employed the same trapping DC voltages across both N_2 and He gas experiments we thought it possible that analyte ions injected into the IM cell filled with helium might be introduced with such force (due to the relative differences in mass between He and N_2) that they do not immediately begin to 'drift' within the IM cell, thus shortening their effective drift length, which would lead to a systematic reduction in CCS_{He} values. However, this effect was not observed for the monomorphic test systems and concanavalin a, which were analysed using identical pre-IM DC voltages to those employed for the other analytes studied.

4. Conclusion and Outlook

Native IM-MS is used to measure a host of protein/protein complexes across many instrumental platforms. Within this study we have shown that, when parameters are tuned to minimise gas-phase activation via the employment of suitable thermometer ions, compact conformations and highly similar structural landscapes can be sampled across three common platforms. These findings in tandem with the body of literature for CCS_{He} values suggests things: 1) that the instrument parameters employed on the 6560 (when operating in He) permit access to native-like dehydrated solution-phase like structures that are notably smaller than those obtained on the G2, or 2) that the instrument parameters employed on the 6560 (when operating in He) promote gas-phase annealing of all but the most rigid structural conformations. When comparing our 6560 CCS_{He} values with the smallest values from the literature (SI Table S9), we observe that our measurements are not systematically smaller, and actually range from ~16% larger to 11% smaller than the smallest $^{DT}CCS_{He}$ values published. As such, we conclude that the smallest CCS_{He} values we observe on the 6560 are most probably dehydrated, native-like solution-phase structures sampled *in vacuo*. Our findings in combination with the broad range of accessed CCS observed within our global CCS frequency histogram plots (and their associated tables) show that proteins/protein complexes are often conformationally flexible, dynamic structures which can easily undergo unintentional gas-phase restructuring to yield non-native conformations. As such, regarding the future of CCS calibration procedures (as utilised to obtain ^{TW}CCS) we propose that the ideal set of calibrants would be monomorphic (and therefore impervious to gas-phase ion activation), unlike proteins. But similar to the array of protein 'standards', these calibrants would span a wide range of masses, mobilities, Δz's and effective densities (thus mimicking the breadth of potential protein samples) whilst being readily available, highly stable and easily sprayed. This version of a calibration approach will be the focus of future studies.

Acknowledgements

This research was supported by the BBSRC (awards: BB/L015048/1, BB/K017802/1 and BB/H013636/1 and the BBSRC/EPSRC-funded Manchester Synthetic Biology Research Centre, SYNBIOCHEM (BB/M017702/1)). MRC, BBSRC, EPSRC, Waters Corp. Agilent and the Universities of Edinburgh and Manchester are thanked for their support of studentships to AF, LGM, and ES.

(1) Smith, D.; Knapman, T.; Campuzano, I.; Malham, R.; Berryman, J.; Radford, S.; Ashcroft, A. Deciphering Drift Time Measurements from Travelling Wave Ion Mobility Spectrometry-Mass Spectrometry Studies. *Eur. J. Mass Spectrom.* **2009**, *15* (5), 113. https://doi.org/10.1255/ejms.947.

(2) Li, J.; Taraszka, J. A.; Counterman, A. E.; Clemmer, D. E. Influence of Solvent Composition and Capillary Temperature on the Conformations of Electrosprayed Ions: Unfolding of Compact Ubiquitin Conformers from Pseudonative and Denatured Solutions. *Int. J. Mass Spectrom.* **1999**, *185*, 37–47. https://doi.org/10.1016/S1387-3806(98)14135-0.

(3) Hudgins, R. R.; Woenckhaus, J.; Jarrold, M. F. High Resolution Ion Mobility Measurements for Gas Phase Proteins: Correlation between Solution Phase and Gas Phase Conformations. *Int. J. Mass Spectrom. Ion Process.* **1997**, *165–166*, 497–507. https://doi.org/10.1016/S0168-1176(97)00182-1.

(4) Breuker, K.; McLafferty, F. W. Stepwise Evolution of Protein Native Structure with Electrospray into the Gas Phase, 10-12 to 102 S. *Proc. Natl. Acad. Sci.* **2008**, *105* (47), 18145–18152. https://doi.org/10.1073/pnas.0807005105.

(5) Wyttenbach, T.; Bowers, M. T. Structural Stability from Solution to the Gas Phase: Native Solution Structure of Ubiquitin Survives Analysis in a Solvent-Free Ion Mobility-Mass Spectrometry Environment. *J. Phys. Chem. B* **2011**, *115* (42), 12266–12275. https://doi.org/10.1021/jp206867a.

(6) Lee, S. W.; Freivogel, P.; Schindler, T.; Beauchamp, J. L. Freeze-Dried Biomolecules: FT-ICR Studies of the Specific Solvation of Functional Groups and Clathrate Formation Observed by the Slow Evaporation of Water from Hydrated Peptides and Model Compounds in the Gas Phase. *J. Am. Chem. Soc.* **1998**, *120* (45), 11758–11765. https://doi.org/10.1021/ja982075x.

(7) McAllister, R. G.; Metwally, H.; Sun, Y.; Konermann, L. Release of Native-like Gaseous Proteins from Electrospray Droplets via the Charged Residue Mechanism: Insights from Molecular Dynamics Simulations. *J. Am. Chem. Soc.* **2015**, *137* (39), 12667–12676. https://doi.org/10.1021/jacs.5b07913.

(8) Wyttenbach, T.; Von Helden, G.; Bowers, M. T. Gas-Phase Conformation of Biological Molecules: Bradykinin. *J. Am. Chem. Soc.* **1996**, *118* (35), 8355–8364. https://doi.org/10.1021/ja9535928.

(9) Florance, H. V.; Stopford, A. P.; Kalapothakis, J. M.; McCullough, B. J.; Bretherick, A.; Barran, P. E. Evidence for α-Helices in the Gas Phase: A Case Study Using Melittin from Honey Bee Venom. *Analyst* **2011**, *136* (17), 3446. https://doi.org/10.1039/c1an15291b.

(10) Shelimov, K. B.; Clemmer, D. E.; Hudgins, R. R.; Jarrold, M. F. Protein Structure in Vacuo: Gas-Phase Conformations of BPTI and Cytochrome C. *J. Am. Chem. Soc.* **1997**, *119* (9), 2240–2248. https://doi.org/10.1021/ja9619059.

(11) Ruotolo, B. T.; Benesch, J. L. P.; Sandercock, A. M.; Hyung, S.-J.; Robinson, C. V. Ion Mobility–Mass Spectrometry Analysis of Large Protein Complexes. *Nat. Protoc.* **2008**, *3* (7), 1139–1152.

https://doi.org/10.1038/nprot.2008.78.

(12) Wang, S. C.; Politis, A.; Di Bartolo, N.; Bavro, V. N.; Tucker, S. J.; Booth, P. J.; Barrera, N. P.; Robinson, C. V. Ion Mobility Mass Spectrometry of Two Tetrameric Membrane Protein Complexes Reveals Compact Structures and Differences in Stability and Packing. *J. Am. Chem. Soc.* **2010**, *132* (44), 15468–15470. https://doi.org/10.1021/ja104312e.

(13) Ruotolo, B. T.; Giles, K.; Campuzano, I. D. G.; Sandercock, A. M.; Bateman, R. H.; Robinson, C. V. Biochemistry: Evidence for Macromolecular Protein Rings in the Absence of Bulk Water. *Science (80-.).* **2005**, *310* (5754), 1658–1661. https://doi.org/10.1126/science.1120177.

(14) Schiffrin, B.; Calabrese, A. N.; Devine, P. W. A.; Harris, S. A.; Ashcroft, A. E.; Brockwell, D. J.; Radford, S. E. Skp Is a Multivalent Chaperone of Outer-Membrane Proteins. *Nat. Struct. Mol. Biol.* **2016**, *23* (9), 786–793. https://doi.org/10.1038/nsmb.3266.

(15) Beveridge, R.; Migas, L. G.; Payne, K. A. P.; Scrutton, N. S.; Leys, D.; Barran, P. E. Mass Spectrometry Locates Local and Allosteric Conformational Changes That Occur on Cofactor Binding. *Nat. Commun.* **2016**, *7*, 1–9. https://doi.org/10.1038/ncomms12163.

(16) Laganowsky, A.; Reading, E.; Allison, T. M.; Ulmschneider, M. B.; Degiacomi, M. T.; Baldwin, A. J.; Robinson, C. V. Membrane Proteins Bind Lipids Selectively to Modulate Their Structure and Function. *Nature* **2014**, *510* (7503), 172–175. https://doi.org/10.1038/nature13419.

(17) Baker, E. S.; Bernstein, S. L.; Gabelica, V.; De Pauw, E.; Bowers, M. T. G-Quadruplexes in Telomeric Repeats Are Conserved in a Solvent-Free Environment. *Int. J. Mass Spectrom.* **2006**, *253* (3), 225–237. https://doi.org/10.1016/j.ijms.2006.03.016.

(18) Gabelica, V.; Baker, E. S.; Teulade-Fichou, M. P.; De Pauw, E.; Bowers, M. T. Stabilization and Structure of Telomeric and C-Myc Region Intramolecular G-Quadruplexes: The Role of Central Cations and Small Planar Ligands. *J. Am. Chem. Soc.* **2007**, *129* (4), 895–904. https://doi.org/10.1021/ja065989p.

(19) Bernstein, S. L.; Dupuis, N. F.; Lazo, N. D.; Wyttenbach, T.; Condron, M. M.; Bitan, G.; Teplow, D. B.; Shea, J. E.; Ruotolo, B. T.; Robinson, C. V.; et al. Amyloid-β 2 Protein Oligomerization and the Importance of Tetramers and Dodecamers in the Aetiology of Alzheimer's Disease. *Nat. Chem.* **2009**, *1* (4), 326–331. https://doi.org/10.1038/nchem.247.

(20) Dupuis, N. F.; Wu, C.; Shea, J. E.; Bowers, M. T. The Amyloid Formation Mechanism in Human IAPP: Dimers Have β-Strand Monomer-Monomer Interfaces. *J. Am. Chem. Soc.* **2011**, *133* (19), 7240–7243. https://doi.org/10.1021/ja1081537.

(21) Gabelica, V.; Shvartsburg, A. A.; Afonso, C.; Barran, P.; Benesch, J. L. P.; Bleiholder, C.; Bowers, M. T.; Bilbao, A.; Bush, M. F.; Campbell, J. L.; et al. Recommendations for Reporting Ion Mobility Mass Spectrometry Measurements. *Mass Spectrom. Rev.* **2019**, 1–30. https://doi.org/10.1002/mas.21585.

(22) Verbeck, G. F.; Ruotolo, B. T.; Gillig, K. J.; Russell, D. H. Resolution Equations for High-Field Ion Mobility. *J. Am. Soc. Mass Spectrom.* **2004**, *15* (9), 1320–1324. https://doi.org/10.1016/j.jasms.2004.06.005.

(23) Mason, E. A.; McDaniel, E. W. *Transport Properties of Ions in Gases*; Wiley: New York, 1988.

(24) Jurneczko, E.; Barran, P. E. How Useful Is Ion Mobility Mass Spectrometry for Structural Biology? The Relationship between Protein Crystal Structures and Their Collision Cross Sections in the Gas Phase.

Analyst **2011**, *136* (1), 20–28. https://doi.org/10.1039/C0AN00373E.

(25) Hernández, H.; Robinson, C. V. Determining the Stoichiometry and Interactions of Macromolecular Assemblies from Mass Spectrometry. *Nat. Protoc.* **2007**, *2* (3), 715–726. https://doi.org/10.1038/nprot.2007.73.

(26) Chen, S. H.; Russell, D. H. How Closely Related Are Conformations of Protein Ions Sampled by IM-MS to Native Solution Structures? *J. Am. Soc. Mass Spectrom.* **2015**, *26* (9), 1433–1443. https://doi.org/10.1007/s13361-015-1191-1.

(27) Jurneczko, E.; Kalapothakis, J.; Campuzano, I. D. G.; Morris, M.; Barran, P. E. Effects of Drift Gas on Collision Cross Sections of a Protein Standard in Linear Drift Tube and Traveling Wave Ion Mobility Mass Spectrometry. *Anal. Chem.* **2012**, *84* (20), 8524–8531. https://doi.org/10.1021/ac301260d.

(28) Valentine, S. J.; Counterman, A. E.; Clemmer, D. E. Conformer-Dependent Proton-Transfer Reactions of Ubiquitin Ions. *J. Am. Soc. Mass Spectrom.* **1997**, *8* (9), 954–961. https://doi.org/10.1016/S1044-0305(97)00085-8.

(29) Merenbloom, S. I.; Flick, T. G.; Williams, E. R. How Hot Are Your Ions in TWAVE Ion Mobility Spectrometry? *J. Am. Soc. Mass Spectrom.* **2012**, *23* (3), 553–562. https://doi.org/10.1007/s13361-011-0313-7.

(30) Gabelica, V.; Livet, S.; Rosu, F.; Bordeaux, U. De; Européen, I.; Chimie, D.; Iecb, B. Optimizing Native Ion Mobility Q-TOF in Helium and Nitrogen for Very Fragile Noncovalent Interactions. **2018**. https://doi.org/10.1007/s13361-018-2029-4.

(31) Paglia, G.; Williams, J. P.; Menikarachchi, L.; Thompson, J. W.; Tyldesley-Worster, R.; Halldórsson, S.; Rolfsson, O.; Moseley, A.; Grant, D.; Langridge, J.; et al. Ion Mobility Derived Collision Cross Sections to Support Metabolomics Applications. *Anal. Chem.* **2014**, *86* (8), 3985–3993. https://doi.org/10.1021/ac500405x.

(32) Paglia, G.; Angel, P.; Williams, J. P.; Richardson, K.; Olivos, H. J.; Thompson, J. W.; Menikarachchi, L.; Lai, S.; Walsh, C.; Moseley, A.; et al. Ion Mobility-Derived Collision Cross Section as an Additional Measure for Lipid Fingerprinting and Identification. *Anal. Chem.* **2015**, *87* (2), 1137–1144. https://doi.org/10.1021/ac503715v.

(33) Stow, S. M.; Causon, T. J.; Zheng, X.; Kurulugama, R. T.; Mairinger, T.; May, J. C.; Rennie, E. E.; Baker, E. S.; Smith, R. D.; McLean, J. A.; et al. An Interlaboratory Evaluation of Drift Tube Ion Mobility-Mass Spectrometry Collision Cross Section Measurements. *Anal. Chem.* **2017**, *89* (17), 9048–9055. https://doi.org/10.1021/acs.analchem.7b01729.

(34) Harrison, J. A.; Kelso, C.; Pukala, T. L.; Beck, J. L. Conditions for Analysis of Native Protein Structures Using Uniform Field Drift Tube Ion Mobility Mass Spectrometry and Characterization of Stable Calibrants for TWIM-MS. *J. Am. Soc. Mass Spectrom.* **2018**. https://doi.org/10.1007/s13361-018-2074-z.

(35) Salbo, R.; Bush, M. F.; Naver, H.; Campuzano, I.; Robinson, C. V.; Pettersson, I.; Jørgensen, T. J. D.; Haselmann, K. F. Traveling-Wave Ion Mobility Mass Spectrometry of Protein Complexes: Accurate Calibrated Collision Cross-Sections of Human Insulin Oligomers. *Rapid Commun. Mass Spectrom.* **2012**,

26 (10), 1181–1193. https://doi.org/10.1002/rcm.6211.

(36) Giles, K.; Williams, J. P.; Campuzano, I. D. G. Enhancements in Travelling Wave Ion Mobility Resolution. In *Rapid Communications in Mass Spectrometry*; 2011; Vol. 25, pp 1559–1566. https://doi.org/10.1002/rcm.5013.

(37) Allen, S. J.; Giles, K.; Gilbert, T.; Bush, M. F. Ion Mobility Mass Spectrometry of Peptide, Protein, and Protein Complex Ions Using a Radio-Frequency Confining Drift Cell. *Analyst* **2016**, *141* (3), 884–891. https://doi.org/10.1039/C5AN02107C.

(38) May, J. C.; Dodds, J. N.; Kurulugama, R. T.; Stafford, G. C.; Fjeldsted, J. C.; McLean, J. A. Broadscale Resolving Power Performance of a High Precision Uniform Field Ion Mobility-Mass Spectrometer. *Analyst* **2015**, *140* (20), 6824–6833. https://doi.org/10.1039/C5AN00923E.

(39) May, J. C.; Goodwin, C. R.; Lareau, N. M.; Leaptrot, K. L.; Morris, C. B.; Kurulugama, R. T.; Mordehai, A.; Klein, C.; Barry, W.; Darland, E.; et al. Conformational Ordering of Biomolecules in the Gas Phase: Nitrogen Collision Cross Sections Measured on a Prototype High Resolution Drift Tube Ion Mobility-Mass Spectrometer. *Anal. Chem.* **2014**, *86* (4), 2107–2116. https://doi.org/10.1021/ac4038448.

(40) Shvartsburg, A. A.; Smith, R. D. Fundamentals of Traveling Wave Ion Mobility Spectrometry. *Anal. Chem.* **2008**, *80* (24), 9689–9699. https://doi.org/10.1021/ac8016295.

(41) Bush, M. F.; Hall, Z.; Giles, K.; Hoyes, J.; Robinson, C. V.; Ruotolo, B. T. Collision Cross Sections of Proteins and Their Complexes: A Calibration Framework and Database for Gas-Phase Structural Biology. *Anal. Chem.* **2010**, *82* (22), 9557–9565. https://doi.org/10.1021/ac1022953.

(42) Wyttenbach, T.; Bowers, M. T. Gas-Phase Conformations: The Ion Mobility/Ion Chromatography Method. *Top. Curr. Chem.* **2003**, *225*, 207–232. https://doi.org/10.1007/b10470.

(43) Migas, L. G.; France, A. P.; Bellina, B.; Barran, P. E. ORIGAMI: A Software Suite for Activated Ion Mobility Mass Spectrometry (AIM-MS) Applied to Multimeric Protein Assemblies. *Int. J. Mass Spectrom.* **2018**, *427*, 20–28. https://doi.org/10.1016/j.ijms.2017.08.014.

(44) Konermann, L. Addressing a Common Misconception: Ammonium Acetate as Neutral PH “Buffer” for Native Electrospray Mass Spectrometry. *J. Am. Soc. Mass Spectrom.* **2017**, *28* (9), 1827–1835. https://doi.org/10.1007/s13361-017-1739-3.

(45) Heck, A. J. R. Native Mass Spectrometry: A Bridge between Interactomics and Structural Biology. *Nat. Methods* **2008**, *5* (11), 927–933. https://doi.org/10.1038/nmeth.1265.

(46) Natalello, A.; Santambrogio, C.; Grandori, R. Are Charge-State Distributions a Reliable Tool Describing Molecular Ensembles of Intrinsically Disordered Proteins by Native MS? *J. Am. Soc. Mass Spectrom.* **2017**, *28* (1), 21–28. https://doi.org/10.1007/s13361-016-1490-1.

(47) Hall, Z.; Robinson, C. V. Do Charge State Signatures Guarantee Protein Conformations? *J. Am. Soc. Mass Spectrom.* **2012**, *23* (7), 1161–1168. https://doi.org/10.1007/s13361-012-0393-z.

(48) Morsa, D.; Gabelica, V.; De Pauw, E. Fragmentation and Isomerization Due to Field Heating in Traveling Wave Ion Mobility Spectrometry. *J. Am. Soc. Mass Spectrom.* **2014**, *25* (8), 1384–1393. https://doi.org/10.1007/s13361-014-0909-9.

(49) Gabellca, V.; De Pauw, E. Internal Energy and Fragmentation of Ions Produced in Electrospray Sources.

Mass Spectrom. Rev. **2005**, *24* (4), 566–587. https://doi.org/10.1002/mas.20027.

(50) Jarrold, M. F. Unfolding, Refolding, and Hydration of Proteins in the Gas Phase. *Acc. Chem. Res.* **1999**, *32* (4), 360–367. https://doi.org/10.1021/ar960081x.

(51) May, J. C.; Jurneczko, E.; Stow, S. M.; Kratochvil, I.; Kalkhof, S.; McLean, J. A. Conformational Landscapes of Ubiquitin, Cytochrome c, and Myoglobin: Uniform Field Ion Mobility Measurements in Helium and Nitrogen Drift Gas. *Int. J. Mass Spectrom.* **2017**, 1–16. https://doi.org/10.1016/j.ijms.2017.09.014.

(52) Beveridge, R.; Covill, S.; Pacholarz, K. J.; Kalapothakis, J. M. D.; Macphee, C. E.; Barran, P. E. A Mass-Spectrometry-Based Framework to Define the Extent of Disorder in Proteins. *Anal. Chem.* **2014**, *86* (22), 10979–10991. https://doi.org/10.1021/ac5027435.

(53) Valentine, S. J.; Counterman, A. E.; Clemmer, D. E. A Database of 660 Peptide Ion Cross Sections: Use of Intrinsic Size Parameters for Bona Fide Predictions of Cross Sections. *J. Am. Soc. Mass Spectrom.* **1999**, *10* (11), 1188–1211. https://doi.org/10.1016/S1044-0305(99)00079-3.

(54) Niu, S.; Ruotolo, B. T. Collisional Unfolding of Multiprotein Complexes Reveals Cooperative Stabilization upon Ligand Binding. *Protein Sci.* **2015**, *24* (8), 1272–1281. https://doi.org/10.1002/pro.2699.

(55) Zhao, Y.; Singh, A.; Xu, Y.; Zong, C.; Zhang, F.; Boons, G. J.; Liu, J.; Linhardt, R. J.; Woods, R. J.; Amster, I. J. Gas-Phase Analysis of the Complex of Fibroblast GrowthFactor 1 with Heparan Sulfate: A Traveling Wave Ion Mobility Spectrometry (TWIMS) and Molecular Modeling Study. *J. Am. Soc. Mass Spectrom.* **2017**, *28* (1), 96–109. https://doi.org/10.1007/s13361-016-1496-8.

(56) Light-Wahl, K. J.; Schwartz, B. L.; Smith, R. D. Observation of the Noncovalent Quaternary Associations of Proteins by Electrospray Ionization Mass Spectrometry. *J. Am. Chem. Soc.* **1994**, *116* (12), 5271–5278. https://doi.org/10.1021/ja00091a035.

(57) Ruotolo, B. T.; Hyung, S. J.; Robinson, P. M.; Giles, K.; Bateman, R. H.; Robinson, C. V. Ion Mobility-Mass Spectrometry Reveals Long-Lived, Unfolded Intermediates in the Dissociation of Protein Complexes. *Angew. Chemie - Int. Ed.* **2007**, *46* (42), 8001–8004. https://doi.org/10.1002/anie.200702161.

(58) Allen, S. J.; Bush, M. F. Radio-Frequency (Rf) Confinement in Ion Mobility Spectrometry: Apparent Mobilities and Effective Temperatures. *J. Am. Soc. Mass Spectrom.* **2016**, *27* (12), 2054–2063. https://doi.org/10.1007/s13361-016-1479-9.

(59) Han, L.; Ruotolo, B. T. Traveling-Wave Ion Mobility-Mass Spectrometry Reveals Additional Mechanistic Details in the Stabilization of Protein Complex Ions through Tuned Salt Additives. *Int. J. Ion Mobil. Spectrom.* **2013**, *16* (1), 41–50. https://doi.org/10.1007/s12127-013-0121-9.

(60) Badman, E. R.; Hoaglund-Hyzer, C. S.; Clemmer, D. E. Monitoring Structural Changes of Proteins in an Ion Trap over 10 - 200 Ms: Unfolding Transitions in Cytochrome c Ions. *Anal. Chem.* **2001**, *73* (24), 6000–6007.

(61) Zhao, Q.; Schieffer, G. M.; Soyk, M. W.; Anderson, T. J.; Houk, R. S.; Badman, E. R. Effects of Ion/Ion Proton Transfer Reactions on Conformation of Gas-Phase Cytochrome c Ions. *J. Am. Soc. Mass Spectrom.* **2010**, *21* (7), 1208–1217. https://doi.org/10.1016/j.jasms.2010.03.032.

(62) Ujma, J.; Giles, K.; Morris, M.; Barran, P. E. New High Resolution Ion Mobility Mass Spectrometer

Capable of Measurements of Collision Cross Sections from 150 to 520 K. *Anal. Chem.* **2016**, *88* (19), 9469–9478. https://doi.org/10.1021/acs.analchem.6b01812.

(63) Pacholarz, K. J.; Barran, P. E. Distinguishing Loss of Structure from Subunit Dissociation for Protein Complexes with Variable Temperature Ion Mobility Mass Spectrometry. *Anal. Chem.* **2015**, *87* (12), 6271–6279. https://doi.org/10.1021/acs.analchem.5b01063.

(64) Allen, S. J.; Eaton, R. M.; Bush, M. F. Analysis of Native-Like Ions Using Structures for Lossless Ion Manipulations. *Anal. Chem.* **2016**, *88* (18), 9118–9126. https://doi.org/10.1021/acs.analchem.6b02089.

(65) Sun, Y.; Vahidi, S.; Sowole, M. A.; Konermann, L. Protein Structural Studies by Traveling Wave Ion Mobility Spectrometry: A Critical Look at Electrospray Sources and Calibration Issues. *J. Am. Soc. Mass Spectrom.* **2016**, *27* (1), 31–40. https://doi.org/10.1007/s13361-015-1244-5.

(66) Jhingree, J. R.; Beveridge, R.; Dickinson, E. R.; Williams, J. P.; Brown, J. M.; Bellina, B.; Barran, P. E. Electron Transfer with No Dissociation Ion Mobility–Mass Spectrometry (ETnoD IM-MS). The Effect of Charge Reduction on Protein Conformation. *Int. J. Mass Spectrom.* **2017**, *413*, 43–51. https://doi.org/10.1016/j.ijms.2016.08.006.

(67) Henderson, S. C.; Li, J.; Counterman, A. E.; Clemmer, D. E. Intrinsic Size Parameters for Val, Ile, Leu, Gln, Thr, Phe, and Trp Residues from Ion Mobility Measurements of Polyamino Acid Ions. *J. Phys. Chem. B* **1999**, *103*, 8780–8785. https://doi.org/10.1021/jp991783h.

(68) Bush, M. F.; Campuzano, I. D. G.; Robinson, C. V. Ion Mobility Mass Spectrometry of Peptide Ions: Effects of Drift Gas and Calibration Strategies. *Anal. Chem.* **2012**, *84* (16), 7124–7130. https://doi.org/10.1021/ac3014498.

(69) Baker, E. S.; Clowers, B. H.; Li, F.; Tang, K.; Tolmachev, A. V.; Prior, D. C.; Belov, M. E.; Smith, R. D. Ion Mobility Spectrometry-Mass Spectrometry Performance Using Electrodynamic Ion Funnels and Elevated Drift Gas Pressures. *J. Am. Soc. Mass Spectrom.* **2007**, *18* (7), 1176–1187. https://doi.org/10.1016/j.jasms.2007.03.031.

(70) Liu, Y.; Valentine, S. J.; Clemmer, D. E. (unpublished results) http://www.indiana.edu/~clemmer.

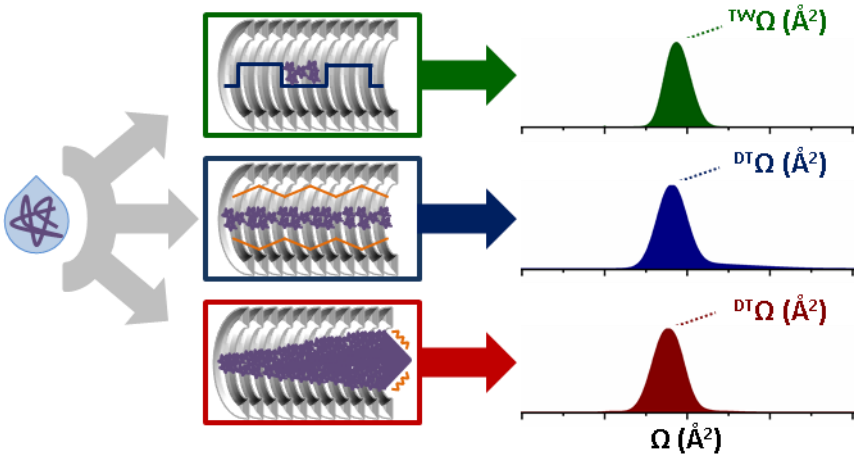

For TOC only